ACS Catalysis

Research Article

pubs.acs.org/acscatalysis

CO Oxidation at the Au/TiO_2 Boundary: The Role of the Au/Ti_{5c} Site

Zhiyao Duan and Graeme Henkelman*

Department of Chemistry and the Institute for Computational Engineering and Sciences, The University of Texas at Austin, Austin, Texas 78712-0165, United States

ABSTRACT: Density functional theory is used to determine the reaction mechanisms of CO oxidation and the active oxygen species on a Au/TiO_2 model catalyst. The model consists of a Au rod supported along the TiO_2 [1$\bar{1}$0] direction of the TiO_2(110) surface. An interfacial Au/Ti_{5c} site at the interface boundary is identified to be particularly active toward O_2 adsorption and dissociation. At this site, O_2 dissociation has an energy barrier of 0.5 eV, which is facile at room temperature. The resulting adsorbed $Au/O/Ti_{5c}$ oxygen species are shown to be stable and active for CO oxidation under relevant reaction conditions with an activation energy of 0.24 eV. Furthermore, the adsorbed $Au/O/Ti_{5c}$ oxygen species functions as an electron reservoir, and it lowers the oxygen vacancy formation energy of a surface lattice oxygen (O_{bri}), as well as the Ti interstitial formation energy, due to electron transfer from high-energy defect states to low-energy *p*-states of the adsorbed $Au/O/Ti_{5c}$ oxygen species. Hence, the O_{bri} species is activated at the oxidized Au/TiO_2 interface boundary and the energy barrier of CO oxidation with O_{bri} is calculated to be 0.55 eV. Thus, the CO oxidation reaction can proceed at room temperature either via a Langmuir–Hinshelwood mechanism with an adsorbed $Au/O/Ti_{5c}$ oxygen species or via a Au-assisted Mars–van Krevelen mechanism with O_{bri}.

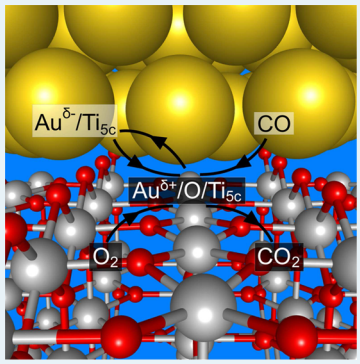

KEYWORDS: *CO oxidation, Au/TiO_2, gold catalysis, heterogeneous catalysis, density functional theory*

1. INTRODUCTION

Oxide-supported Au nanoparticle catalysts have attracted enormous interest because they exhibit high activity for a number of different reactions.[1−4] CO oxidation on TiO_2 supported Au nanoparticles catalysts (Au/TiO_2) has received the most intense investigation to elucidate the origin of the high catalytic activity at low temperature. However, due to the complex nature of the metal–oxide interface, there is a lack of consensus regarding several essential aspects of this reaction. The most important debate is the nature of the active site, and especially the site responsible for O_2 activation, which is the most energy intensive elementary step. In recent reviews,[5,6] various proposed active sites are summarized. The list includes metallic Au,[7,8] cationic Au,[9,10] under-coordinated Au,[11−13] and perimeter sites at the interface between the Au nanoparticle and the TiO_2 support.[14−16]

Recent studies have provided new insights understanding toward the nature of the active site. Green et al. found that CO oxidation occurs at the exposed metal–support interface at low temperature (T = 120 K) using IR spectroscopy.[17] The accompanying density function theory (DFT) calculations further assign the active site of O_2 activation to be the dual (Au–Ti) site at the interface boundary. The reaction mechanism is resolved to be that of adsorbed molecular O_2 reacting with adsorbed CO on the TiO_2 surface via a coadsorption CO–O_2 complex. In a number of theoretical studies,[18−21] molecularly adsorbed O_2 is also identified as an active oxygen species. However, desorption of the molecular O_2 is observed at 170 K in the work by Stiehl et al.,[22,23] indicating a different CO oxidation reaction mechanism at the higher reaction temperatures of relevance.

Based on multipulse measurements performed in a temporal analysis of products (TAP) reactor at temperature between 353 and 673 K, Behm and co-workers have identified the active oxygen species to be atomic surface lattice oxygen at the perimeter of Au nanoparticles.[24−26] Accordingly, the reaction mechanism is determined to be a Au-assisted Mars–van Krevelen (MvK) mechanism, in which surface lattice oxygen at, or close to, perimeter sites is consumed by coupling with CO and replenished by O_2 dissociative adsorption. A recent theoretical study by the Hammer group supports the Au-assisted MvK mechanism and further points out that only the surface lattice oxygen along the [1$\bar{1}$0] direction of the support is catalytically active, and not along the [001] direction.[27] It remains unclear, however, how the Au nanoparticle activates the surface lattice oxygen: are active metal–support interactions at the interface playing a role, or does Au provide anchoring sites for CO so that it can react with nearby surface lattice oxygen? Furthermore, the experimental assignment of the active oxygen species in these studies is based on macroscopic observations and not directly from characterization methods with atomic resolution, so it is possible that the active role of other oxygen species has been overlooked.

This study addresses the electronic structure of the Au/TiO_2 interface and the adsorption and dissociation of O_2 at the interface. We have found that O_2 dissociation is facile at an electron-rich Au/Ti_{5c} site at the interface boundary. The resulting adsorbed atomic oxygen at the Au/Ti_{5c} site is stable

Received: October 17, 2014
Revised: January 21, 2015
Published: January 29, 2015

DOI: 10.1021/cs501610a
ACS Catal. 2015, 5, 1589−1595

under typical reaction conditions and active toward CO oxidation. This atomic oxygen species is also found to play a role in activating surface lattice oxygen at the interface perimeter.

2. COMPUTATIONAL METHODS

Plane-wave based spin-polarized DFT calculations were performed using the Vienna Ab initio Simulation Package.[28−30] The generalized gradient approximation with the Perdew−Wang (PW91) functional[31] was used to describe the exchange and correlation energy. Electron−ion interactions were treated by the projector augmented wave method.[32] In all calculations, the energy cutoff of the plane wave basis set was 400 eV. The DFT+U method was applied to 3d orbitals of Ti to correct the on-site Coulomb interactions.[33] The value of U_{eff} was chosen to be 4.0 eV to reproduce the electronic structure that has been observed experimentally.[34,35] Due to the large model employed, a Γ point sampling of the Brillouin zone was used to calculate the total energy of the system. Optimized structures were obtained by minimizing the forces on each ion until they fell below 0.05 eV/Å. Transition states were determined with the climbing image nudged elastic band method.[36,37] A Bader analysis was employed to determine the local charge of atoms in the system.[38−40]

3. RESULTS AND DISCUSSION

3.1. Model of the Au/TiO_2 Interface. The interface a TiO_2 supported Au nanoparticle is modeled by a periodic one-dimensional Au rod deposited along the TiO_2 $[1\bar{1}0]$ direction of a rutile $TiO_2(110)$ slab. In a previous study,[18] a Au rod was placed along the [001] direction on the TiO_2 substrate in order to minimize the lattice mismatch between Au and the substrate, and to minimize the system size required. However, recent environmental transmission electron microscopy measurements have shown that the dominant surface direction of the interface perimeter is along the ⟨110⟩ direction.[41] Accordingly, we orient the Au rod along the $[1\bar{1}0]$ direction in order to be consistent with the experimental observation, even though the lattice mismatch between Au and the TiO_2 substrate is greater in this direction. The model employed throughout this study is shown in Figure 1. The Au rod contains three layers; the interfacial layer has the structure of the Au(111) surface. In order to minimize the strain, a long Au rod consisting of seven Au atoms along the $[1\bar{1}0]$ direction is used. The lattice constants calculated in this work are a = 4.17 Å for fcc Au and a = 4.69 Å, c = 3.03 Å for rutile TiO_2. Based on these lattice constants, the Au rod is compressed by 3.7% in the axial direction to be commensurate with the $p(5 \times 3)$ $TiO_2(110)$ substrate in the $[1\bar{1}0]$ direction. The TiO_2 substrate contains three stoichiometric TiO_2 layers. The top TiO_2 layer is allowed to relax while the bottom two layers are fixed in bulk lattice positions.

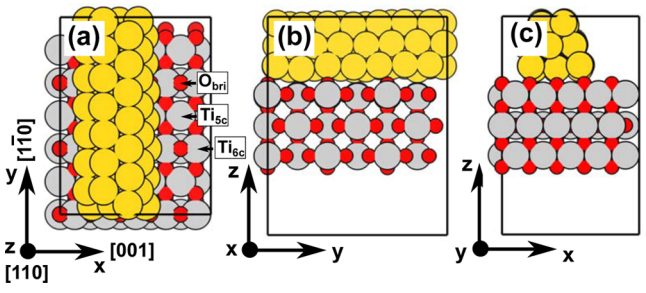

Figure 1. Au rod supported on the rutile $TiO_2(110)$ surface: (a) top, (b) front, and (c) side views. The bridging oxygen, the coordinatively unsaturated Ti site, and the coordinatively saturated Ti site on the $TiO_2(110)$ surface are denoted as O_{bri}, Ti_{5c}, and Ti_{6c}.

3.2. Electronic Structure of the Au/TiO_2 Interface. Understanding the electronic structure of the Au/TiO_2 interface is important for elucidating the exceptional catalytic activity of the Au/TiO_2 catalyst, given that its constituents are catalytically inert, individually. When an interface is formed between a metal and a nonreactive (strongly ionic) oxide, interfacial electronic states appear primarily due to three types of interactions. The first effect is the conventional metal-induced gap states (MIGS), which are produced by the exponential decay of delocalized metal states within the insulator.[42,43] The characteristic of the conventional MIGS is a structureless continuum of states in the band gap of the oxide substrate. The second cause of interfacial states is the metal−oxygen bonding at the interface.[44,45] The metal−oxygen interaction results in donor- and acceptor-like states at well-defined energies located close the valence band maximum (VBM) and the conduction band minimum (CBM) of the oxide.[46] The third effect is the polarization of metal electrons by the electronic field of the substrate.[47,48] The polarization is analogous to the macroscopic image charge effect. As a result, metal electrons will populate/deplete the space between the deposited metal and the surface cation/anion. The interfacial states from the conventional MIGS and the metal−oxygen hybridization induce charge transfer across the interface creating an interface dipole moment. Polarization of the metal electrons also contributes to the interface dipole moment, although it does not involve any charge transfer across the interface. The work function of the metal and the oxide is shifted according to the direction of the interface dipole moment.

The projected density of states (pDOS) of the Au rod and the TiO_2 slab before and after interface formation are shown in Figure 2a,b. When separated, the Fermi energy (E_f) of the Au rod is higher than the CBM of the TiO_2 slab, so that electrons flow from the Au rod to the TiO_2 substrate, making the oxide negatively charged. The negatively charged oxide is also manifest by the occupation of acceptor-like states near the CBM due to the metal−oxygen hybridization at the interface, as

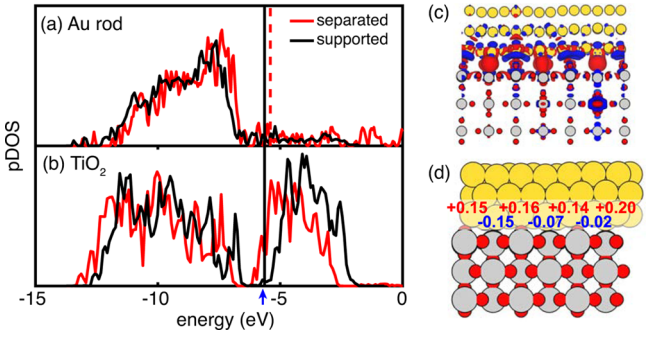

Figure 2. Projected density of states (pDOS) of the (a) Au rod and (b) TiO_2 substrate before and after the Au is supported on the TiO_2 substrate. The electronic energy reference is the vacuum level in both cases. The charge redistribution due to the interface formation is plotted in (c), where red indicates electron accumulation and blue indicates electron depletion. The net bader charges of the Au atoms along the interface boundary are shown (d).

DOI: 10.1021/cs501610a
ACS Catal. 2015, 5, 1589−1595

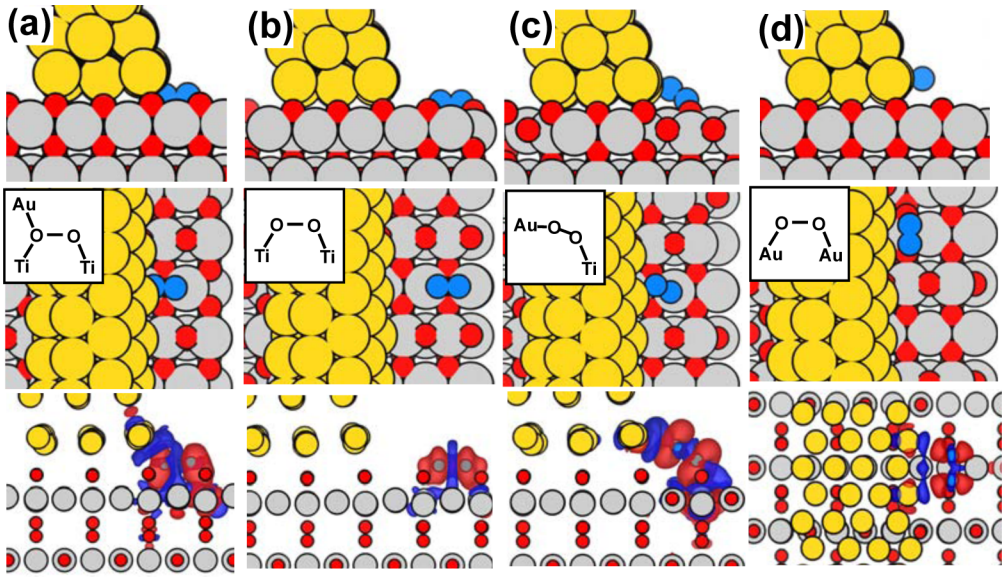

Figure 3. Structures of adsorbed O_2 (top and middle panels) and the charge redistribution upon O_2 adsorption (bottom) at different adsorption sites at the perimeter of the Au/TiO_2 interface boundary: (a) $Au/Ti_{5c}–Ti_{5c}$, (b) $Ti_{5c}–Ti_{5c}$, (c) Au– Ti_{5c}, (d) Au–Au. The side and top views of the adsorption structures are shown in the top and middle panels, respectively. In this figure and in later figures, Au, Ti, and O atoms are represented by yellow, gray, red circles, respectively; adsorbed O_2 is cyan.

Table 1. Properties of Adsorbed O_2 at Different Sites at the Perimeter of the Au/TiO_2 Interface Boundary and the Bare TiO_2 Surface, Including Bond Length, Net Charge, Magnetization, Binding and Dissociation Energies, and Activation Energy for Dissociation

site	bond (Å)	charge (|e|)	mag. (μ_B)	E_{bind} (eV)	E_{diss} (eV)	E_a (eV)
$Au/Ti_{5c}–Ti_{5c}$	1.429	0.92	0.00	−1.64	−0.70	0.50
$Ti_{5c}–Ti_{5c}$	1.401	0.82	0.00	−1.31	0.04	1.16
$Au–Ti_{5c}$	1.370	0.72	0.00	−1.05	−0.13	—
Au–Au	1.278	0.32	0.62	0.04	0.18	—
$Ti_{5c}–Ti_{5c}$ bare TiO_2	1.261	0.00	1.98	−0.06	3.53	—

indicated by the blue arrow in Figure 2b. Charge transfer from Au to the stoichiometric TiO_2 support is also observed in experimental measurements by photoelectron spectroscopy.[49,50] Beside charge transfer caused by the work function difference of the metal and the oxide, polarization effects at the interface also contribute to the band alignment. In order to resolve the polarization effect, the charge redistribution upon interface formation is shown in Figure 2c. It can be seen that electron density is depleted from the space between Au and O_{bri} and populated into the space between Au and Ti_{5c}, as a result of the polarization of metal electrons induced by the electrostatic field of the substrate, or equivalently, the image charge effect. Consequently, Au atoms of two different charge states can be identified along the interface boundary. The Bader charges in Figure 2d show that cationic Au is present at the Au/O_{bri} site and anionic Au is present at the Au/Ti_{5c} site.

In summary, the interface established between the Au rod and the TiO_2 substrate gives rise to two main effects. First, excess electrons appear on the TiO_2 substrate as a result of the charge transfer from the Au rod. Second, both cationic and anionic Au species appear at the interface depending on their registry with the substrate due to the image charge effect. These two effects, caused by interface formation, will be shown to have significant consequences for the catalytic properties.

3.3. O_2 Adsorption and Dissociation at the Au/TiO_2 Interface. To investigate the catalytic properties of the Au/TiO_2 interface, we start by studying O_2 adsorption. Four unique O_2 adsorption sites ($Au/Ti_{5c}–Ti_{5c}$, $Ti_{5c}–Ti_{5c}$, Au– Ti_{5c}, Au–Au) are recognized at the interface perimeter, as well as a $Ti_{5c}–Ti_{5c}$ site on bare rutile $TiO_2(110)$ surface, for comparison. The O_2 adsorption structures are shown in Figure 3, and their corresponding properties are summarized in Table 1.

The O_2 molecule adsorbs strongly at the interface with binding energies greater than 1 eV. This is in sharp contrast with the weak O_2 adsorption on the bare TiO_2 surface, illustrating the prominent role of the Au/TiO_2 interface. To understand the reason behind the binding strength enhancement at the interface, Bader charges and magnetic moments of the adsorbed O_2 are calculated. Adsorbed O_2 at the $Au/Ti_{5c}–Ti_{5c}$, $Ti_{5c}–Ti_{5c}$, and Au– Ti_{5c} sites all feature a significant charge enrichment and a singlet spin state, which suggest a charge transfer to the LUMO (lowest unoccupied molecular orbital) $2\pi^*$ states of O_2 and a charge state similar to a peroxide (O_2^{2-}) species. Charge transfer to the LUMO $2\pi^*$ states is also seen in the plots of charge density redistribution upon O_2 adsorption in Figure 3, where electrons populate the LUMO $2\pi^*$ orbital in a dumbbell shape when O_2 is adsorbed at the $Au/Ti_{5c}–Ti_{5c}$, $Ti_{5c}–Ti_{5c}$, and Au– Ti_{5c} sites. In contrast, on the bare TiO_2 surface, no charge is transferred to O_2, and it has a triplet spin state, which is a signature of the gas-phase O_2 molecule. The most pronounced charge transfer to O_2, and also the strongest binding, occur at the $Au/Ti_{5c}–Ti_{5c}$ site. At this adsorption state, O_2 not only accepts charge from the substrate, it also benefits from the electron-rich Au/Ti_{5c} site. O_2 does not

DOI: 10.1021/cs501610a
ACS Catal. 2015, 5, 1589–1595

adsorb at Au−Au sites because the Au−O interaction is of a covalent nature, and there is no significant charge transfer to the $2\pi^*$ state of O_2.

To understand why charge transfers to adsorbed O_2, the *p*-states of O_2 in the gas-phase and various adsorbed states are shown in Figure 4. Initially, the LUMO $2\pi^*$ state in the gas-phase O_2 lies above the Fermi level of the Au/TiO_2 interface. When O_2 is brought into contact with the bare TiO_2 surface, the LUMO $2\pi^*$ state is shifted downward in energy because of the electrostatic interaction with the Ti cation. The energy shift of the O_2 orbitals can be seen in Figure 4a,b. As a result of this shift, the charge transfer to the LUMO $2\pi^*$ states is now possible because it drops below the Fermi level of the Au/TiO_2 interface.

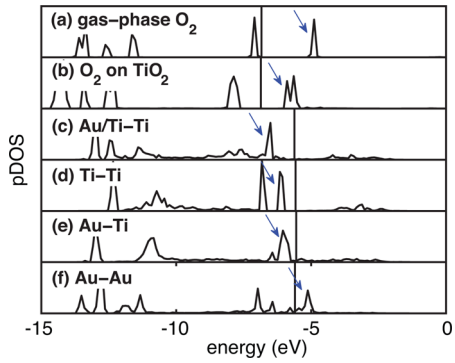

Figure 4. pDOS of an O_2 molecule in (a) gas-phase and adsorbed at the (b) bare TiO_2 surface, (c) $Au/Ti_{5c}-Ti_{5c}$, (d) $Ti_{5c}-Ti_{5c}$, (e) $Au-Ti_{5c}$, and (f) Au−Au sites. The Fermi level of each system is denoted by a black vertical line. The LUMO $2\pi^*$ orbital of O_2 is indicated by a blue arrow.

In addition, adsorbed O_2 must be in contact with the Ti cation in order to gain access to the excess electron density on the substrate transferred from the Au rod. After charge transfer, the occupied LUMO $2\pi^*$ state is further stabilized by the Ti cations in which O_2 is in contact. The degree of stabilization positively correlates with the number of electrons transferred to the LUMO $2\pi^*$ state, as can be seen in Figure 4c−e. This picture of charge transfer to the $2\pi^*$ state is similar to that described in a previous study by Liu et al.[20]

The strong binding of O_2 at the Au/TiO_2 interface suggests the possibility of facile dissociation. The heats of O_2 dissociation (E_{diss}) and the activation energies (E_a) at the $Au/Ti_{5c}-Ti_{5c}$, $Ti_{5c}-Ti_{5c}$, and $Au-Ti_{5c}$ sites are listed in Table 1. The dissociation process is exothermic by −0.7 eV, and the energy barrier is 0.5 eV at the $Au/Ti_{5c}-Ti_{5c}$ site, as can also be seen in the minimum energy path (MEP) in Figure 5. After dissociation, one O atom is further embedded into the space between the Au atom and the Ti_{5c} atom; the other O atom sits atop the Ti_{5c} atom. The dissociation of the O_2 molecule adsorbed at the $Ti_{5c}-Ti_{5c}$ site, on the other hand, is endothermic and has an energy barrier of 1.16 eV. At the $Au-Ti_{5c}$ site, O_2 dissociation is found to proceed in two steps; first, O_2 diffuses to the $Au/Ti_{5c}-Ti_{5c}$ site and then dissociates, as in Figure 5. The charge redistribution in the final state is shown in Figure 5, where charge transfer to the two adsorbed O atoms can be seen. A Bader analysis gives net charges on O at the Au/Ti_{5c} and Ti_{5c} sites of 0.87*e* and 0.74*e*, respectively. Both have zero magnetic moments as in a O^{2-} species. The source of the excess charge on the two O atoms is different, however. At the Au/Ti_{5c} site, the Au electrons that initially populated the space between Au and Ti_{5c} now populate the O *p*-states. The excess electron density on the O atom atop the Ti_{5c} site comes from the oxide substrate initially transferred from the Au rod. The additional interaction between the adsorbed O and Au at the Au/Ti_{5c} site makes its binding energy lower than that of the adsorbed O atop the Ti_{5c} site by 0.4 eV.

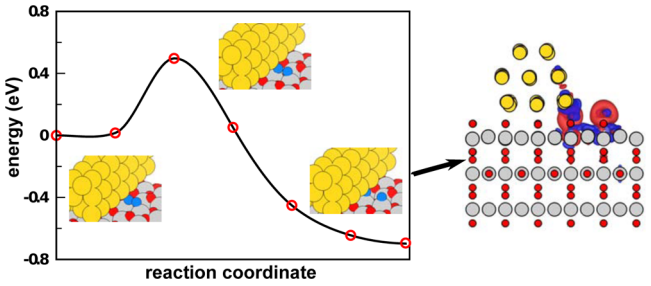

Figure 5. MEP of O_2 dissociation at the $Au/Ti_{5c}-Ti_{5c}$ site of the Au/TiO_2 interface boundary. The insets show the atomic structure of the initial, transition, and final states. The right panel shows the charge redistribution upon adsorption of the two atomic O atoms.

3.4. Oxidation of Au/TiO_2 Interface. Interfacial oxidation is expected under catalytically relevant conditions because of facile O_2 dissociation. To account for the oxidation, we have conducted ab initio thermodynamics calculations to determine the Gibbs free energy of O adsorption (ΔG_O^{ads}) as a function of the O chemical potential (μ_O), calculated as[51]

$$\Delta G_O^{ads} \approx E_{Au/TiO_2+N_O\cdot O} - E_{Au/TiO_2} - N_O\left(\frac{1}{2}E_{O_2} + \Delta\mu_O\right) \quad (1)$$

where $E_{Au/TiO_2+N_O\cdot O}$ is the total energy of the oxidized Au/TiO_2 interface with N_O oxygen atoms adsorbed around the interface perimeter, $E_{Au/Ti}O_2$ is the total energy of the Au/TiO_2 interface, E_{O_2} is the total energy of gas-phase O_2 molecule, and $\Delta\mu_O$ is the free energy contribution to μ_O. In these calculations, various O adsorption sites are considered including the Au/Ti_{5c} site at the interface, the Au/Ti_{5c} site at the interface boundary, and Ti_{5c} sites away from the interface. Based on these different O adsorption sites, six oxidized Au/TiO_2 structures are examined in the ab initio thermodynamics calculation. The Gibbs free energy of oxygen adsorption as a function of O chemical potential is shown in Figure 6, along with the adsorption structures.

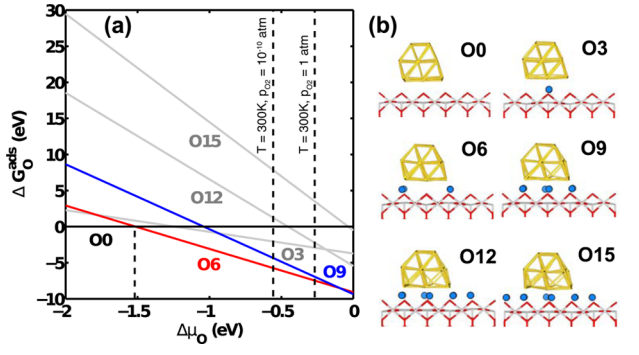

Figure 6. (a) Gibbs free energy of adsorption is plotted as a function of oxygen chemical potential. (b) O adsorption structures at the Au/TiO_2 interface perimeter.

DOI: 10.1021/cs501610a
ACS Catal. 2015, 5, 1589−1595

Structures with a reduced TiO_2 substrate containing oxygen vacancies are not included because our calculations, as well as previous theoretical studies,[52] have shown that the reduced structures are unstable under an oxygen-rich environment. We also note that a reduced TiO_2 slab with Ti interstitials could have a strong influence on the interfacial oxidation, because Ti interstitials induced donor-like gap states and provide the electrons required for O_2 adsorption and dissociation, as pointed out in ref 53. In this study, however, we focus on the interfacial oxidation of pristine TiO_2 slab.

Figure 6a shows that over a wide range of μ_O values, the O6 structure is most stable, in which O atoms adsorb at the Au/Ti_{5c} sites along the interface boundary. More importantly, the O6 stability region extends to the experimental low-temperature oxidation reaction conditions (T = 300 K, $p_{O2} = 10^{-10}$–1 atm), as indicated in Figure 6a by vertical dashed lines. At extremely high μ_O, close to the point of O_2 condensation ($\Delta\mu_O$ = 0), the oxidation of the entire Au/TiO_2 interface can occur; the corresponding structure is shown as O9. In contrast, O atoms occupying Ti_{5c} sites at the interface perimeter are energetically favorable over the whole range of $\Delta\mu_O$ examined. Most importantly, the adsorbed O atoms at the Au/TiO_2 interface boundary are the most abundant O species under reaction conditions. Interfacial oxidation at the Au/Ti_{5c} site has been recognized in previous theoretical studies.[52,54] More recently, using an evolutionary global optimization algorithm, full interfacial oxidation structures (like the O9 structure) are predicted to be the most stable under catalytically relevant conditions.[27,55] This discrepancy may be related to the different optimization algorithm employed (global vs local).

3.5. Promoting Effect of Interfacial Oxygen on TiO_2 Reduction. In the most catalytically relevant O6 structure, the previously mentioned anionic Au species above the Ti_{5c} site along the interface boundary is oxidized and turned into cationic Au. The net Bader charges on the Au atoms along the interface boundary are shown in Figure 7a. Another effect of

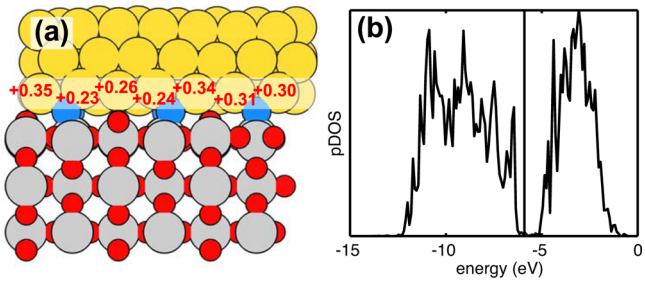

Figure 7. (a) Net Bader charges and (b) pDOS of the Au atoms along the oxidized Au/TiO_2 interface perimeter of the O6 structure.

the oxidation of the interface boundary is that additional electronic states appear in the band gap, as shown in Figure 7b. The additional states leads to a shift of the Fermi level from the CBM in Figure 2b to slightly above the VBM. As a result of the Fermi level shift, we found that reduction of the TiO_2 slab is promoted.

At the Au/stoichiometric TiO_2 interface boundary (the O0 structure), the vacancy formation energy of a surface lattice oxygen (O_{bri}) is calculated to be 3.18 eV. Compared to the vacancy formation energy of 2.33 eV on the bare TiO_2 surface, Au is found to stabilize O_{bri}. At the oxidized Au/TiO_2 interface (the O6 structure), the oxygen vacancy formation energy of O_{bri} is reduced to 1.57 eV. Similarly, TiO_2 reduction is also enhanced by the presence of Ti interstitials. The Ti interstitial formation energy is calculated to be 0.98 and −0.71 eV for the O0 and O6 structures, respectively, by placing a Ti atom into an O-octahedral site between the first and second layer of the TiO_2 slab. Metallic Ti is used as the reference for the Ti interstitial defect, and the chemical potential of Ti with respect to this reference is taken to be 0. Based upon the spin density, the charge state of the Ti interstitial defect is 0 and +3 at the stoichiometric and oxidized interfaces, respectively. This decrease in the oxygen vacancy and the Ti interstitial formation energy can be explained by the shift of Fermi level between stoichiometric Au/TiO_2 and oxidized Au/TiO_2, as shown in Figure 7. Experimental observations and theoretical calculations indicate that oxygen vacancy and Ti interstitial defect produce a localized state right below the conduction band.[53,56] At the stoichiometric Au/TiO_2 interface, the localized defect states are occupied, because the Fermi level is located around the CBM. In contrast, at the oxidized Au/TiO_2 interface, it is energetically favorable for the electrons to be released from the high-energy defect states and occupy states near the Fermi level around the VBM, resulting in a stabilization of the vacancy. These states at the Fermi level around VBM of the oxidized Au/TiO_2 interface are p-states of the adsorbed Au/O/Ti_{5c} oxygen species.

To summarize, we argue that the TiO_2 support can be more easily reduced under catalytically relevant conditions due to the presence of interfacial oxygens at Au/Ti_{5c} sites. Evidence from experiments support this prediction. In situ electrical conductance measurements[57] have shown that the electrical conductance of the Au/TiO_2 catalyst increases immediately after the introduction of the reaction mixture, which is attributed to the generation of oxygen vacancies at the perimeter of the interface boundary. Ti interstitial ions are found to exist at the interface of Au/TiO_2 from TEM images, whereas they are deficient in a peripheral region of the gold nanoparticles.[58] This observation can be explained by the Ti interstitials in the bulk diffusing to the Au/TiO_2 interface because of the low defect formation energies.

3.6. O Species Active for CO Oxidation. As shown in the previous sections, O_2 can readily overcome the 0.5 eV dissociation barrier at the Au/Ti_{5c}–Ti_{5c} adsorption site at room temperature. Additionally, the dissociated atomic O is stable at the Au/Ti_{5c} site under reaction conditions, as demonstrated by our ab initio thermodynamic calculations. Finally, we consider the ability for O adsorbed at the Au/Ti_{5c} site to oxidize CO, which in turn readily adsorbs to the Au nanoparticle. Figure 8 shows the MEP of this reaction and that the process is highly exothermic with a calculated activation

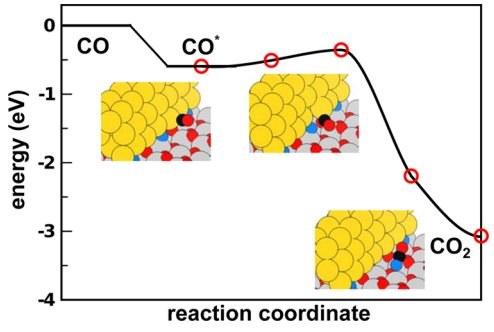

Figure 8. MEP of adsorbed O at the Au/Ti_{5c} site reacting with a CO adsorbed on the Au rod. The insets show the atomic structure of the initial, transition, and final states.

DOI: 10.1021/cs501610a
ACS Catal. 2015, 5, 1589–1595

energy of 0.24 eV. The low activation energy indicates that the adsorbed O at the Au/Ti_{5c} site is highly active toward CO oxidation.

Previous experimental studies using TAP[25] have assigned the active oxygen species to be surface lattice oxygen (O_{bri}) at the perimeter of Au nanoparticle. Our computational results, however, suggest that the active role of adsorbed O at the Au/Ti_{5c} site (Au/O/Ti_{5c}) at the interface boundary has been overlooked in the interpretation of the experimental results, because the criteria for the active oxygen species summarized from the experimental observation are met by the Au/O/Ti_{5c} species. First, deposition of Au/O/Ti_{5c} is fast through facile O_2 dissociation at Au/Ti_{5c}−Ti_{5c} site. Second, Au/O/Ti_{5c} is stable provided that the average adsorption energy of Au/O/Ti_{5c} is −1.51 eV/O in the O6 structure. Third, Au is indispensable in O_2 dissociation and stabilizing Au/O/Ti_{5c}.

A further issue in the assignment of Au/O/Ti_{5c} as the active oxygen species is a comparison with the activity of the O_{bri} species at the interface boundary. As demonstrated in the previous section, interfacial oxygen at the Au/Ti_{5c} site reduces the O vacancy formation energy of O_{bri}. To further illustrate the role of the Au/O/Ti_{5c} oxygen species in activating surface lattice oxygens (O_{bri}), MEPs for the CO oxidation involving an O_{bri} at the interface boundary with and without the adsorbed Au/O/Ti_{5c} oxygen species were calculated and the results are shown in Figure 9. The MEP of CO oxidation can be

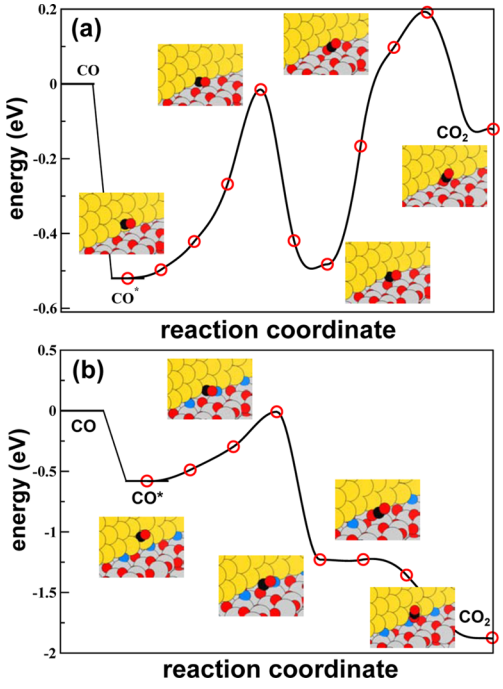

Figure 9. MEP of a surface O_{bri} reacting with an adsorbed CO on the Au rod in (a) O0 and (b) oxidized O6 structures.

considered consisting of two parts. In the first step, adsorbed CO on the Au rod diffuses toward the O_{bri} and then forms an intermediate bent CO_2 species. To complete the CO oxidation, in the second step, the bent CO_2 desorbs from the interface boundary leaving behind an oxygen vacancy. In the bent CO_2 formation process, the barrier is about 0.55 eV at both the oxidized and stoichiometric interface boundaries. The activation of the interfacial O_{bri} species is manifested in the CO_2 desorption step. At the Au/stoichiometric TiO_2 interface boundary, the desorption is endothermic with a barrier 0.65 eV, due to the high vacancy formation energy of O_{bri}. In sharp contrast, the CO_2 desorption process is exothermic and barely activated at the oxidized interface boundary. Hence, we have shown that surface lattice oxygen (O_{bri}) is also active toward CO oxidation under reaction conditions. The activation of O_{bri} relies on the presence of adsorbed Au/O/Ti_{5c} oxygen species. In experiments, the activity of surface lattice oxygens toward CO oxidation is confirmed by in situ electrical conductance measurement.[57] It was found the electrical conductance of the Au/TiO_2 catalyst immediately increased just after the introduction of the reaction mixture, which is attributed to the generation of oxygen vacancies at the perimeter of the interface boundary.

In this study, we have proposed a new picture of the CO oxidation reaction mechanism over a Au/TiO_2 catalyst. Both the Langmuir−Hinshelwood (LH) and Au-assisted MvK mechanisms are calculated to be active at the Au/TiO_2 interface boundary. Briefly, adsorbed CO on the Au rod can either react with an adsorbed Au/O/Ti_{5c} oxygen species via a LH mechanism or react with a surface lattice oxygen O_{bri} via a Au-assisted MvK mechanism at the oxidized Au/TiO_2 interface boundary. Although the LH mechanism has been extensively explored theoretically, in contrast to this work, most previous calculations predict that CO reacts with molecular O_2 forming an intermediate CO·O_2 complex from which CO_2 forms and desorbs.[18,20,21,59,60] This mechanism of CO oxidation could be active at low temperatures, but it is not consistent with recent experiments showing that the active oxygen species is atomic oxygen, due to its superior stability at room temperature and above.[25] More recently, Hammer's group highlighted the role of the Au/Ti_{5c} site for adsorbing oxygen species and explicitly proposed that adsorbed O_2 and O are active for CO oxidation.[27] This reaction mechanism is similar to our LH mechanism, but the activity of O_{bri} was not examined. For the Au-assisted MvK mechanism, the activity of O_{bri} was investigated and confirmed in a recent ab initio molecular dynamics study using the small Au_{16} cluster model.[61]

3.7. Role of Au/Ti_{5c} Site in CO Oxidation. The Au/Ti_{5c} site at the interface boundary of Au/stoichiometric TiO_2 is electron-rich and oxophilic due to the polarization effect of Ti cations on the metallic Au orbitals. We have demonstrated that O_2 adsorption, dissociation, and Au/TiO_2 interface oxidation can take place at this Au/Ti_{5c} site. In terms of CO oxidation via the LH mechanism, the Au/Ti_{5c} site stores oxygen for CO to react with. During the course of the CO oxidation process via the LH mechanism, the Au atom alternates between anionic and cationic state. For the Au-assisted MvK mechanism, the Au/Ti_{5c} site participates in the reaction only indirectly in that the adsorbed O at the site works as an electron reservoir which facilitates oxygen vacancy generation.

4. CONCLUSION

We have employed DFT calculations to investigate CO oxidation at the Au/TiO_2 interface perimeter along the TiO_2 [1$\bar{1}$0] direction. Further understanding has been gained regarding the exceptional catalytic activity of CO oxidation at room temperature. We have identified the Au/Ti_{5c} site at the interface boundary as being is active for O_2 dissociation. At the Au/Ti_{5c} site, O_2 dissociatively adsorbs with with an energy barrier of 0.5 eV. Under reaction conditions, the Au/Ti_{5c} site is found to be oxidized. Interfacial oxygen atoms facilitate the reduction of the TiO_2 support either by oxygen vacancy

DOI: 10.1021/cs501610a
ACS Catal. 2015, 5, 1589−1595

formation or Ti interstitial formation. The adsorbed O atom at the Au/Ti_{5c} is shown to be active toward CO oxidation with a low energy barrier of 0.24 eV. In contrast, surface lattice oxygen O_{bri} at an unoxidized interface boundary is inactive. At the oxidized interface boundary, however, O_{bri} is activated by adsorbed Au/O/Ti_{5c} oxygen.

AUTHOR INFORMATION

Corresponding Author

*E-mail: henkelman@utexas.edu.

Notes

The authors declare no competing financial interest.

ACKNOWLEDGMENTS

This work is supported by the Department of Energy under contract DE-FG02-13ER16428 and the Welch Foundation under grant F-1841. The calculations were done at the National Energy Research Scientific Computing Center and the Texas Advanced Computing Center.

REFERENCES

(1) Haruta, M.; Daté, M. *Appl. Catal., A* **2001**, *222*, 427−437.
(2) Haruta, M. *CATTECH* **2002**, *6*, 102−115.
(3) Bond, G. C.; Thompson, D. T. *Gold Bulletin* **2000**, *33*, 41−50.
(4) Hashmi, A. S. K.; Hutchings, G. J. *Angew. Chem., Int. Ed.* **2006**, *45*, 7896−7936.
(5) Haruta, M. *Faraday Discuss.* **2011**, *152*, 11−32.
(6) Wu, Y. Y.; Mashayekhi, N. A.; Kung, H. H. *Catal. Sci. Technol.* **2013**, *3*, 2881−2891.
(7) Yang, J. H.; Henao, J. D.; Raphulu, M. C.; Wang, Y.; Caputo, T.; Groszek, A. J.; Kung, M. C.; Scurrell, M. S.; Miller, J. T.; Kung, H. H. *J. Phys. Chem. B* **2005**, *109*, 10319−10326.
(8) Kung, M. C.; Davis, R. J.; Kung, H. H. *J. Phys. Chem. C* **2007**, *111*, 11767−11775.
(9) Fierro-Gonzalez, J. C.; Gates, B. C. *Chem. Soc. Rev.* **2008**, *37*, 2127−2134.
(10) Miller, J.; Kropf, A.; Zha, Y.; Regalbuto, J.; Delannoy, L.; Louis, C.; Bus, E.; van Bokhoven, J. *J. Catal.* **2006**, *240*, 222−234.
(11) Mavrikakis, M.; Stoltze, P.; Nørskov, J. K. *Catal. Lett.* **2000**, *64*, 101−106.
(12) Lopez, N.; Janssens, T.; Clausen, B.; Xu, Y.; Mavrikakis, M.; Bligaard, T.; Nørskov, J. K. *J. Catal.* **2004**, *223*, 232−235.
(13) Lopez, N.; Nørskov, J. K. *J. Am. Chem. Soc.* **2002**, *124*, 11262−11263.
(14) Schubert, M. M.; Hackenberg, S.; van Veen, A. C.; Muhler, M.; Plzak, V.; Behm, R. *J. Catal.* **2001**, *197*, 113−122.
(15) Kung, H. H.; Kung, M. C.; Costello, C. K. *J. Catal.* **2003**, *216*, 425−432.
(16) Bond, G. C.; Thompson, D. T. *Catal. Rev.* **1999**, *41*, 319−388.
(17) Green, I. X.; Tang, W.; Neurock, M.; Yates, J. T. *Science* **2011**, *333*, 736−739.
(18) Molina, L. M.; Rasmussen, M. D.; Hammer, B. *J. Chem. Phys.* **2004**, *120*, 7673−7680.
(19) Wang, J. G.; Hammer, B. *Phys. Rev. Lett.* **2006**, *97*, 136107.
(20) Liu, Z.-P.; Gong, X.-Q.; Kohanoff, J.; Sanchez, C.; Hu, P. *Phys. Rev. Lett.* **2003**, *91*, 266102.
(21) Wang, Y.-G.; Yoon, Y.; Glezakou, V.-A.; Li, J.; Rousseau, R. *J. Am. Chem. Soc.* **2013**, *135*, 10673−10683.
(22) Stiehl, J. D.; Kim, T. S.; McClure, S. M.; Mullins, C. B. *J. Am. Chem. Soc.* **2004**, *126*, 1606−1607.
(23) Stiehl, J. D.; Kim, T. S.; McClure, S. M.; Mullins, C. B. *J. Am. Chem. Soc.* **2004**, *126*, 13574−13575.
(24) Kotobuki, M.; Leppelt, R.; Hansgen, D. A.; Widmann, D.; Behm, R. J. *J. Catal.* **2009**, *264*, 67−76.
(25) Widmann, D.; Behm, R. J. *Angew. Chem., Int. Ed.* **2011**, *50*, 10241−10245.
(26) Widmann, D.; Behm, R. J. *Acc. Chem. Res.* **2014**, *47*, 740−749.
(27) Vilhelmsen, L. B.; Hammer, B. *ACS Catal.* **2014**, *4*, 1626−1631.
(28) Kresse, G.; Hafner, J. *Phys. Rev. B* **1993**, *47*, 558.
(29) Kresse, G.; Furthmüller, J. *Comput. Mater. Sci.* **1996**, *6*, 15−50.
(30) Kresse, G.; Furthmüller, J. *Phys. Rev. B* **1996**, *54*, 11169.
(31) Perdew, J. P.; Wang, Y. *Phys. Rev. B* **1992**, *45*, 13244.
(32) Blöchl, P. E. *Phys. Rev. B* **1994**, *50*, 17953.
(33) Dudarev, S. L.; Botton, G. A.; Savrasov, S. Y.; Humphreys, C. J.; Sutton, A. P. *Phys. Rev. B* **1998**, *57*, 1505−1509.
(34) Morgan, B. J.; Watson, G. W. *Surf. Sci.* **2007**, *601*, 5034−5041.
(35) Finazzi, E.; Di Valentin, C.; Pacchioni, G.; Selloni, A. *J. Chem. Phys.* **2008**, *129*, 154113.
(36) Henkelman, G.; Jónsson, H. *J. Chem. Phys.* **2000**, *113*, 9978−9985.
(37) Henkelman, G.; Uberuaga, B. P.; Jónsson, H. *J. Chem. Phys.* **2000**, *113*, 9901−9904.
(38) Bader, R. F. W. *Atoms in Molecules: A Quantum Theory*; Oxford University Press: New York, 1990.
(39) Henkelman, G.; Arnaldsson, A.; Jónsson, H. *Comput. Mater. Sci.* **2006**, *36*, 354−360.
(40) Tang, W.; Sanville, E.; Henkelman, G. *J. Phys.: Condens. Matter* **2009**, *21*, 084204.
(41) Kuwauchi, Y.; Yoshida, H.; Akita, T.; Haruta, M.; Takeda, S. *Angew. Chem., Int. Ed.* **2012**, *51*, 7729−7733.
(42) Louie, S. G.; Cohen, M. L. *Phys. Rev. B* **1976**, *13*, 2461−2469.
(43) Bordier, G.; Noguera, C. *Phys. Rev. B* **1991**, *44*, 6361−6371.
(44) Tung, R. T. *Phys. Rev. B* **2001**, *64*, 205310.
(45) Goniakowski, J.; Noguera, C. *Interface Sci.* **2004**, *12*, 93−103.
(46) Yeo, Y.-C.; King, T.-J.; Hu, C. *J. Appl. Phys.* **2002**, *92*, 7266−7271.
(47) Goniakowski, J. *Phys. Rev. B* **1998**, *57*, 1935−1941.
(48) Giordano, L.; Cinquini, F.; Pacchioni, G. *Phys. Rev. B* **2006**, *73*, 045414.
(49) Okazawa, T.; Kohyama, M.; Kido, Y. *Surf. Sci.* **2006**, *600*, 4430−4437.
(50) Jiang, Z.; Zhang, W.; Jin, L.; Yang, X.; Xu, F.; Zhu, J.; Huang, W. *J. Phys. Chem. C* **2007**, *111*, 12434−12439.
(51) Reuter, K.; Scheffler, M. *Phys. Rev. B* **2001**, *65*, 035406.
(52) Laursen, S.; Linic, S. *J. Phys. Chem. C* **2009**, *113*, 6689−6693.
(53) Wendt, S.; Sprunger, P. T.; Lira, E.; Madsen, G. K. H.; Li, Z.; Hansen, J. Ø.; Matthiesen, J.; Blekinge-Rasmussen, A.; Lægsgaard, E.; Hammer, B.; Besenbacher, F. *Science* **2008**, *320*, 1755−1759.
(54) Laursen, S.; Linic, S. *Phys. Chem. Chem. Phys.* **2009**, *11*, 11006−11012.
(55) Vilhelmsen, L. B.; Hammer, B. *J. Chem. Phys.* **2013**, *139*, 204701.
(56) Henrich, V. E.; Dresselhaus, G.; Zeiger, H. J. *Phys. Rev. Lett.* **1976**, *36*, 1335−1339.
(57) Maeda, Y.; Iizuka, Y.; Kohyama, M. *J. Am. Chem. Soc.* **2013**, *135*, 906−909.
(58) Tanaka, T.; Sumiya, A.; Sawada, H.; Kondo, Y.; Takayanagi, K. *Surf. Sci.* **2014**, *619*, 39−43.
(59) Remediakis, I. N.; Lopez, N.; Nørskov, J. K. *Angew. Chem.* **2005**, *117*, 1858−1860.
(60) Li, L.; Gao, Y.; Li, H.; Zhao, Y.; Pei, Y.; Chen, Z.; Zeng, X. C. *J. Am. Chem. Soc.* **2013**, *135*, 19336−19346.
(61) Li, L.; Zeng, X. C. *J. Am. Chem. Soc.* **2014**, *136*, 15857−15860.

DOI: 10.1021/cs501610a
ACS Catal. 2015, 5, 1589−1595